# Supporting Information

## Zhang et al. 10.1073/pnas.1419553111

### SI Materials and Methods

**Clinical History and Phenotype.** A family of Turkish origin came to attention because of congenital deafness and QT interval prolongation in two of six children (Fig. S1*A*). The father (carrier$^{478\text{-}2A/T}$, #14) was completely asymptomatic, even during competitive sport. His hearing was normal; a 12-lead ECG showed normal baseline repolarization (QTc: 400 ms) and T-wave morphology. His wife (#16), who shared the same great-grandparents with her husband, also had normal ECG (QTc: 421 ms) and hearing. The parents had four children. Their first child, a daughter (#18), was admitted because of congenital inner ear deafness, recurrent syncope during exercise, and a very long QT interval (QTc: 600 ms), together with negative T-waves. Based on these findings, the diagnosis of JLNS was made. She was treated with bilateral cochlea implants, a body weight-adjusted β-blocker and a pacemaker implantation; however, at the age of 8 y, she died suddenly during adrenergic stress. Their second child, a son (JLNS$^{478\text{-}2T/T}$, #19), also had typical JLNS with congenital deafness, an extremely long QT interval (QTc: up to 700 ms after birth, later 570 ms), and recurrent syncope during high-dose β-blocker therapy. At the age of 7 y, an implantable cardioverter defibrillator (ICD) was implanted for secondary prevention. In the following 4 y, he experienced a series of appropriate ICD shocks due to ventricular fibrillation, requiring the first exchange of the ICD system at 11 y. In the following years, in particular during exercise and cycling, he continued to receive further ICD therapies. So far, a cochlear implantation has not been performed. Because of recurrent cardiac events and therapy, he became increasingly psychologically traumatized. The complete coding sequences of *KCNQ1* and flanking intronic sequences (~25 bp at each site) were analyzed by direct sequencing. In concordance with the recessive disease trait, an intronic mutation (c.478-2A>T) leading to a predicted nonfunctional KCNQ1 protein was identified in a heterozygous state in both parents and found to be homozygous in the affected children (Fig. 1*A* and Fig. S1*A*).

In case of the c.1781G>A *KCNQ1* mutation, QT prolongation was identified in a 69-y-old female patient (QTc; Bazett Eq. 506 ms) (Fig. S1*B*). By sequence screening, the missense heterozygous mutation c.1781G>A was found in exon 15 of the *KCNQ1* gene, thus leading to the diagnosis of LQT1 syndrome (Fig. 1*A*). The patient (LQT1$^{1781G/A}$) is asymptomatic, but she is being treated with β-blockers.

**Generation of Patient-Specific hiPSCs.** Fibroblasts were obtained from skin punch biopsies from patients carrying the mutations (JLNS$^{478\text{-}2T/T}$, carrier$^{478\text{-}2A/T}$, and LQT1$^{1781G/A}$) and from a wild-type healthy female individual (wt2), after written informed consent and following approval by the Münster (c.478-2A>T) and Leiden (c.1781G>A and wt2) University ethics committees. Male control fibroblasts (wt1) were obtained from the ATCC tissue culture collection (CRL-2097). Fibroblasts that migrated out of the dermis tissue were cultured until passage 3 and used for reprogramming. One hundred thousand fibroblasts were infected with 5 multiplicities of infection (MOI) of the replication-defective and persistent Sendai virus (1) (or Life Technologies A1378001), carrying the four transcription factors *OCT4*, *SOX2*, *KLF4*, and *MYC* and either cultured on mouse embryonic fibroblasts or, alternatively, on gelatin-coated dishes by using conventional KSR/FGF2-containing hESC medium with 0.5 mM valproic acid. In case of the c.1781G>A lines, after 1 wk, primary colonies, resembling mouse embryonic stem cell colonies, appeared. These colonies were dissociated with TrypleE Select 1x (Gibco Life Technologies) and repeatedly transfected with siRNA interfering with viral RNA-dependent RNA polymerase to silence the Sendai virus (1). After an additional 14 d, emerging hiPSC colonies were picked and expanded. In case of the c.478-2A>T lines, hiPSC clones were picked from the primary plates, expanded, and loss of Sendai viruses was monitored over several passages. Erasure of the virus was confirmed by qPCR using specific primers (Table S1). An independent set of hiPSC lines was generated from the c.478-2A>T fibroblasts by using a conventional retroviral approach. Details about the latter procedure and assays used for characterization of resulting hiPSC lines were described (2).

**Genetic Engineering of hiPSC Lines.** For generating an isogenic pair of wt and JLNS$^{478\text{-}2T/T}$-like hESCs, the intron 2-exon 3 boundary of *KCNQ1* was targeted by using a double-nicking CRISPR/Cas-9n approach (3). Oligonucleotide sequences defining the target sites in this genomic region are given in Table S1. These oligonucleotides were phosphorylated, annealed in pairs, and cloned into a modified version of the pX335 plasmid (Addgene 42335) carrying a GFP-Puromycin selection cassette (4). HuES6 hESCs were cotransfected with both CRISPR vectors and transiently selected for 48 h by using 0.4 μg/mL puromycin to enrich for transfected cells. Following replating of cells at clonal dilution, single clones were picked ~2 wk later to be analyzed for deletion mutations at the intron 2-exon 3 boundary by using nested gPCR (primer pairs KCNQ1 CRISPR screen 1 and 2; Table S1). PCR products were mixed at a 1:1 ratio with wt fragments, denatured at 95 °C, and reannealed by slow cooling to 25 °C. For mutation detection, five units of T7 Endonuclease I (NEB M0302S) were added to the PCR products to be incubated for 15 min at 37 °C. hESC clones showing digestion products on agarose gels—which indicates mutations within the PCR fragment—were expanded. For analysis of homozygous hESC clones, PCR fragments of clonal lines were TOPO TA-cloned and sequenced (10 TOPO clones per line to statistically obtain sequence information on both alleles).

For generating an isogenic pair of heterozygous and homozygous c.1781G>A-mutated hiPSCs, the *KCNQ1* locus in the LQT1$^{1781G/A}$ hiPSCs was modified in a stepwise manner by recombineering, as described (5, 6). Briefly, a BAC containing ~181 kb of the human *KCNQ1* locus was modified by inserting 1 kb downstream of the mutation site a *loxP*-flanked positive selection cassette (*NeoR*) comprising of a mammalian promoter (*pGK*), a bacterial promoter (*gb3*), and a G418/kanamycin-resistance gene (*Neo*). A 14.7-kb fragment, including a 10.6-kb 5′-homology arm, the inserted *NeoR*-resistance cassette, and a 2-kb 3′-homology arm, was then subcloned into a minimal vector (Gene Bridges), generating the wt *KCNQ1* targeting vector. The c.1781G>A mutation was inserted in the wt vector by using the QuikChange XL Site-Directed Mutagenesis Kit (Agilent Technologies). The mutated vector was linearized with the restriction enzyme NotI before electroporation (7). Targeted clones were identified by using a PCR-based screening strategy. The introduction of the c.1781A > G *KCNQ1* mutation in the targeted clones was confirmed by sequencing. The *loxP*-flanked G418-resistance cassette was excised by using Cre recombinase. The homozygous mutated hiPSC line was then subcloned, and clonal lines were screened for the loss of the Neor*R* cassette. Karyotype analysis was performed by using COBRA-FISH as described (8). Twenty metaphase spreads for each sample were analyzed.

For functionally complementing JLNS$^{478T/T}$ hiPSCs using an inducible transgene approach, wt *KCNQ1* cDNA was amplified from a preexisting vector (KCNQ1-psGEM) by using primer pairs KCNQ1 full cl (Table S1) and subcloned into the MluI/SpeI sites of expression vector KA0717 (gift from Kenjiro Adachi, Max Planck Institute for Molecular Biomedicine, Münster; Fig. S4*F*). This construct was cotransfected with transactivator and transposase-encoding vectors (KA0637 and SBI Biosciences PB200PA-1) into JLNS$^{478T/T}$ hiPSCs by using FuGENE HD (Roche; ratio 10:1:3). Stable transgene-positive clones were selected by using G418. One selected clone was expanded and verified to up-regulate *KCNQ1* upon doxycycline (DOX) (0.3–3 μg/mL) administration.

**Genomic Sequencing and Monitoring of *KCNQ1* Imprinting Status.** Genomic DNA was isolated from cultured cells by using the Gentra PureGene cell kit (Qiagen) or ethanol precipitation of SDS/Proteinase K-lysed cells. To confirm the presence of the heterozygous and the homozygous c.1781G>A and c.478-2A>T *KCNQ1* mutations, regions surrounding the lesion sites were amplified from genomic DNA by using conventional PCR (Table S1), purified using the QIAquick PCR Purification kit (Qiagen), and sequenced.

To investigate the imprinting status of *KCNQ1* in undifferentiated hiPSCs and cardiomyocytes (CMs) derived from these, a region surrounding the informative SNP rs1057128 were amplified by RT-PCR using primers given in Table S1 (KCNQ1 rs1057128), TOPO TA-cloned (Life Technologies), and sequenced on a clonal basis.

**Culture of hiPSCs and Differentiation into the Cardiac Lineage.** hiPSC lines were maintained in culture by using standard procedures (9) or under feeder-free conditions in FTDA medium (10). Cardiac differentiation was induced by using a monolayer protocol. Briefly, at day −1, $2 \times 10^4$ cells per cm$^2$ were plated on matrigel-treated plates. At day 0 of differentiation, a mixture of cytokines (20 ng/mL BMP4, R&D; 20 ng/mL Activin A, Miltenyi Biotec; and 1.5 μM GSK3 inhibitor CHIR99021, Axon Medchem) was added to the cells to induce mesoderm formation. After 3 d, the cytokines were removed and a Wnt inhibitor (5 μM, XAV939, TOCRIS) was added for 3 d (11). Medium was further changed every 3–4 d. Alternatively, differentiation was induced upon replating single cell-dissociated hiPSCs to form embryoid bodies (EBs) or as monolayers by using 0.5–2 ng/mL BMP4, 1 μM CHIR99021, and 20 ng/mL FGF2 (R&D) for 24 h. This treatment was followed by incubation with 2 μM IWP-2 (Santa Cruz) from days 2 to 3, in insulin-free KO-DMEM (Life Technologies) with transferrin-selenium and 250 μM sodium ascorbate. Twenty- to thirty-d-old CMs were dissociated for immunofluorescence and for single cell electrophysiology by using Tryple Select 1x (Gibco Life Technologies). Dissociated CMs were plated on fibronectin- or matrigel-coated 10-mm glass coverslips in APEL medium. Alternatively, beating monolayers were single cell-dissociated after 2 wk by using Papain (Worthington)/Accutase (Merck Millipore), allowed to reform high-density beating sheets on fibronectin/gelatin and further maturate in B27/KO-DMEM (Life Technologies). For transferring cells onto Matrigel/gelatin-coated MEAs in B27, either monolayers were partially digested by using Acctuase or beating EBs from suspension cultures were directly transferred onto the electrodes and allowed to attach overnight. Further details about these procedures are available upon request.

**Gene Expression Analysis.** Total RNA was isolated from undifferentiated and differentiated cells at different time points, using the RNeasy Mini kit (Qiagen), following the manufacturer's instructions. One microgram of RNA was reverse transcribed by using the iScript-cDNA Synthesis kit (Bio-Rad) or M-MLV (Affymetrix) with $dT_{15}$ priming. Expression profiles of genes of interest were determined by qPCR using the iQ or iTaq Universal SYBR Green Supermixes (Bio-Rad). Gene expression was normalized to *GAPDH*, *TNNT2*, or *RPL37A*/*RPS16*. Results were either analyzed by using the ΔCt or ΔΔCt methods or represented as heat maps by using GENE-E software (www.broadinstitute.org/cancer/software/GENE-E/index.html). Primers are listed in Table S1.

For genome-wide expression analysis, total RNA was isolated from undifferentiated hiPSCs by using Macherey-Nagel NucleoSpin mRNA or Qiagen RNeasy kits with on-column DNA digestion. Five hundred nanograms of RNA were used as input for biotin-labeled cRNA synthesis by using the linear TotalPrep RNA Amplification kit (Ambion). The biotinylated cRNA was quantified and quality-checked on RNA Nano chips on a 2100 Bioanalyzer (Agilent). Hybridizations were conducted on Human HT12v4 Expression BeadChip arrays (Illumina) as recommended by the manufacturer. Hybridized arrays were scanned on HiScanSQ instrumentation (Illumina) by using default settings. Raw microarray data were analyzed with the PluriTest algorithm (www.pluritest.org) (12).

**Immunofluorescence and Western Blot Analysis.** For immunofluorescence analysis, cells were fixed in 4% paraformaldehyde, permeabilized with phosphate buffer saline (PBS)/0.1% Triton-X 100 (Sigma-Aldrich), and blocked with 10% (vol/vol) FCS (Life Technologies). Samples were incubated overnight at 4 °C with the following primary antibodies: NANOG ([1:20], goat polyclonal; R&D Systems), SSEA4 and OCT4 ([1:100], mouse monoclonal and [1:100], goat polyclonal, respectively; both from Santa Cruz), TRA1-81 ([1:100], mouse monoclonal; Millipore), AFP ([1:500], mouse monoclonal; Sigma), SMA ([1:100], mouse monoclonal; DakoCytomation), βIII Tubulin ([1:1,000], mouse monoclonal; Sigma), MLC2v ([1:200], rabbit polyclonal; ProteinTech Group), MLC2a ([1:400], mouse monoclonal; Synaptic Systems), α-ACTININ ([1:800], mouse monoclonal; Sigma–Aldrich), TNNI3 ([1:500], rabbit polyclonal; Santa Cruz), and KCNE1 ([1:50], mouse polyclonal; Abcam). For KCNQ1 staining ([1:50], mouse monoclonal or [1:100] rabbit polyclonal; both from Abcam), cells were permeabilized with PBS/0.05% Tween (Merck) and blocked with 5% (wt/vol) BSA. Alternatively, KCNQ1 ([1:100], rabbit polyclonal; Santa Cruz) was stained following fixation with ice-cold Acetone/Methanol. Primary antibodies were detected with either Cy3- or Alexa Fluor-conjugated antibodies. Nuclei were visualized with DAPI (Invitrogen) and F-actin with Phalloidin-Alexa-Fluor-488-conjugate ([1:40]; Invitrogen). Images were captured by using either Leica DMI6000-AF6000/Zeiss Axiovert fluorescence microscopes or a Leica SP5 confocal laser-scanning microscope.

Western blot analysis was performed on whole cell extract from CMs according to standard protocols. Briefly, cells were lysed in 1% Nonidet P-40, 150 mM NaCl, 10% (vol/vol) glycerol, 5 mM EDTA, and 50 mM Tris·HCl at pH 7.4; 80 μg of protein was loaded on 10% (vol/vol) acrylamide gels and blotted onto PVDF or nitrocellulose membranes. The antibodies used were as follows: KCNQ1 ([1:200], mouse monoclonal; Abcam, or [1:500], rabbit polyclonal; Alomone Labs), TNNI3 ([1:500], rabbit polyclonal; Santa Cruz), KCNE1 ([1:50], rabbit polyclonal; Alomone Labs), and GAPDH ([1:2,500], rabbit polyclonal; Abcam). Primary antibodies were detected with HRP-conjugated secondary antibodies and revealed with Super Signal West Pico Chemiluminescent Substrate (Thermo Scientific).

**Cellular Electrophysiology.**

***Data acquisition and analysis.*** APs, $I_{Ks}$, and $I_{Kr}$ were recorded with the amphotericin-perforated patch-clamp technique by using an Axopatch 200B Clamp amplifier (Molecular Devices) 7 d after dissociation. Coverslips containing the hiPSC-CMs were put in a recording chamber on the stage of an inverted microscope and superfused with modified Tyrode's solution (36 ± 0.2 °C) containing the following (in mM): NaCl 140, KCl 5.4, $CaCl_2$ 1.8,

$MgCl_2$ 1.0, glucose 5.5, and Hepes 5.0; pH 7.4 (NaOH). Intrinsically quiescent hiPSC-CMs that were able to contract upon field stimulation were selected for measurements. Patch pipettes (borosilicate glass; resistance 2–3 MΩ) were filled with (in mM): K-gluconate 125, KCl 20, NaCl 10, amphotericin-B 0.22, Hepes 10, pH 7.2 KOH. APs were low-pass filtered (10 kHz) and digitized (40 kHz), whereas $I_{Ks}$ and $I_{Kr}$ were filtered and digitized at 2 and 5 kHz, respectively. Potentials were corrected for the estimated liquid junction potential (13). Cell membrane capacitance ($C_m$) was estimated as described (14). Series resistance was compensated for by at least 80%. Voltage control, data acquisition, and analysis were accomplished by using custom software.

***AP measurements.*** APs were elicited at 0.5–4 Hz by 3-ms, ∼1.2× threshold current pulses through the patch pipette. We analyzed RMP, APA, PlaA (defined as the potential difference between RMP and potential 20 ms after the upstroke), $dV/dt_{max}$, $APD_{20}$, $APD_{50}$, and $APD_{90}$. Data from 10 consecutive APs were averaged.

***$I_{Ks}$ and $I_{Kr}$ measurements.*** $I_{Ks}$ and $I_{Kr}$ were activated upon 1-s depolarizing pulses from a holding potential of −60 mV in the presence of 5 μM nifedipine to block the L-type $Ca^{2+}$ current. $I_{Ks}$ was measured as 0.5 μM JNJ303-sensitive current, whereas $I_{Kr}$ was measured as 5 μM E4031-sensitive current in the presence of 0.5 μM JNJ303. Current densities were calculated by dividing current amplitudes by $C_m$. $I_{Ks}$ in hiPSC-CMs have typically small current densities (15); therefore, to reliably measure $I_{Ks}$, we have selected large single cells (average $C_m$: 55.9 ± 10.2 pF, $n = 33$).

Alternatively, in a minority of experiments, JNJ303-sensitive currents were recorded in whole-cell mode of patch clamp technique by using an EPC10 amplifier (HEKA Elektronik, Lambrecht/Pfalz). Patch pipettes (borosilicate glass; resistance 5–8 MΩ) were filled with intracellular solution (in mM): K-gluconate 125, KCl 20, NaCl 5, Hepes 10, pH 7.2 KOH. $I_{Ks}$ was activated upon 2 s (wt1) or 5 s (carrier and JLNS) voltage pulses to +40 MV from a holding potential of –80 mV. During recordings, cells were first superfused with Tyrode's solution (room temperature) containing 0.1% DMSO followed by application of 1 μM JNJ303.

***MEA measurements.*** For electrophysiological analysis on multielectrode arrays (USB-MEA256 system, Multichannel Systems), dried 9-well or 256-electrode MEAs were coated on the electrode area with a small droplet of 1:75 prediluted Matrigel mixed with 0.2% gelatin for at least 2 h at room temperature. EBs or single cell/cell aggregate CMs were plated onto these surfaces as described above, in B27/KO-DMEM or 2% (vol/vol) FCS/KO-DMEM. FPD measurements of spontaneous electrical activity were typically initiated ∼2 d after plating. Preferably, ground state potentials were recorded by using EBs/larger cell aggregates, whereas effects of drugs were typically monitored from beating monolayers/smaller aggregates (to ensure improved penetrance of molecules). In case of monitoring drug effects on FPD, recordings were initiated after a 10- to 20-min wash-in incubation at 37 °C. Wash-out recordings were performed after at least five media changes. $T_{max}$ and peak-to-peak finding algorithms were implemented in MC Rack software v4.5.7. Only FP spectra showing a clear $T_{max}$-like signal were considered. $QT_{max}$ intervals and beating frequencies were averaged from five consecutive measurements, extracted from multiple independent recordings, and data processed in Microsoft Excel by using Bazett's formula for frequency correction: $cQT_{max} = QT_{max}\ (ms)/(RR\ (s))^{0.5}$. Only samples showing beat intervals in the range of ∼700–2,300 ms were considered for $QT_{max}$ quantification, and Bazett's formula was validated to faithfully normalize QT values within this interval. FP curves monitoring drug responses were overlayed in Adobe Photoshop.

***Measurements in* Xenopus *oocytes.*** For evaluating channel currents mediated by wt and mutant KCNQ1 in *Xenopus laevis* oocytes, *KCNQ1* in expression vector psGEM was modified to harbor an exon 3 deletion following amplification and subcloning of a cDNA fragment from $JLNS^{478\text{-}2T/T}$ CMs (primers KCNQ1 span ex3 cl; Table S1). The G1781A mutant was generated by using the Site-Directed Mutagenesis Kit (Agilent Technologies) and confirmed by sequencing. *KCNE1* was in vector psp64. Poly-A–capped mRNA was synthesized by using a mMessage mMachine kit (Ambion). Single oocytes (EcoCyte Bioscience) were injected with a nanoliter injector 2000 (World Precision Instruments) with 32 nL of (*i*) *KCNQ1* wt (5 ng) + *KCNE1* (1 μg); (*ii*) *KCNQ1* mutant (5 ng) + *KCNE1* (1 μg); (*iii*) *KCNQ1* wt + *KCNQ1* mutant + *KCNE1* (to mimic heterozygous CMs); or (*iv*) *KCNE1* alone (1 μg, as negative control). Injected oocytes were incubated at 18 °C in Barth's solution. Two-electrode voltage clamp recordings were performed by using a Turbo Tec-10CD (NPI) amplifier with Digidata 1322A AD/DA interface and pCLAMP 9.0 software (Axon Instruments/Molecular Devices). Recording pipettes were filled with 3 M KCl and had resistances of 0.5–2 MΩ. Channel currents were recorded 3 d after injection at room temperature in ND96 recording solution. KCNQ1/KCNE1 channel currents were elicited with 5-s pulses from potentials of −100 to +60 mV in 20-mV increments, starting from holding potentials of −80 mV. Data were analyzed with Clampfit 9.0 and Prism 4 software. Currents were normalized to values at 60 mV of the control current.

**Analysis of KCNQ1 Trafficking.** Analysis of KCNQ1 trafficking in *Xenopus* oocytes was based on a preexisting psGEM vector containing a *KCNQ1-GFP* fusion transgene. The c.1781G>A mutation was introduced by using Site-Directed Mutagenesis Kit (Agilent Technologies). Equal amounts of wt or mutant *KCNQ1-GFP* mRNA were coinjected with *KCNE1* into *Xenopus* oocytes, as described above. Fluorescent images were taken 2 d later by using confocal microscopy (Zeiss LSM 700). Confocal images were analyzed by using ImageJ software. Briefly, green pixel brightness was assumed to be proportional to local KCNQ1-GFP concentration at the oocyte outer membrane. Green intensity values (eight-bit scale) were extracted for all image pixels to create corresponding histograms for all independently injected cells ($n = 10$ per transgene). Pixel numbers in each category were multiplied with their corresponding relative GFP intensities and then summed up from arbitrary threshold GFP intensity onwards. This procedure was validated to result in total GFP intensity values that were roughly proportional to the amount of injected *KCNQ1-GFP* mRNA.

**Molecular Dynamic Simulations of KCNQ1 wt and KCNQ1 R594Q.** Molecular dynamic (MD) simulations were based on the model by Strutz-Seebohm et al. (16) from which a 30-aa peptide surrounding the mutation site was extracted (KCNQ1 residues 573–603). Residue R594 is positioned in a crevice formed by a loop in the model. For simulations of the R594Q mutation the residue was mutated in silico. MD simulations were performed by using Yasara Structure software using a described protocol (17). In brief, MD parameters used were as follows: force field, AMBER03; temperature, 298K; pressure, 1 bar; pH, 7.0; Coulomb electrostatics, cutoff 7.86; NaCl, 0.9%; solvent density, 0.997; time steps, 2 fs. Average structures were determined from 5-ns simulations. The rmsd and structural folds were calculated by using Yasara scripts md_analyze.mcr and md_analyzesecstr.mcr, respectively.

**Statistics.** Data are presented as mean ± SEM. Groups were compared by using one-way ANOVA followed by Tukey's test or two-way repeated measures ANOVA followed by pairwise comparison using the Student-Newman-Keuls test. MEA data were analyzed on the basis of two-sided unpaired Student *t* tests. Statistical significance is indicated by symbols *, &, and # ($P < 0.05$).

1. Nishimura K, et al. (2011) Development of defective and persistent Sendai virus vector: A unique gene delivery/expression system ideal for cell reprogramming. *J Biol Chem* 286(6):4760–4771.
2. Greber B, et al. (2011) FGF signalling inhibits neural induction in human embryonic stem cells. *EMBO J* 30(24):4874–4884.
3. Ran FA, et al. (2013) Double nicking by RNA-guided CRISPR Cas9 for enhanced genome editing specificity. *Cell* 154(6):1380–1389.
4. Cong L, et al. (2013) Multiplex genome engineering using CRISPR/Cas systems. *Science* 339(6121):819–823.
5. Fu J, Teucher M, Anastassiadis K, Skarnes W, Stewart AF (2010) A recombineering pipeline to make conditional targeting constructs. *Methods Enzymol* 477: 125–144.
6. Bellin M, et al. (2013) Isogenic human pluripotent stem cell pairs reveal the role of a KCNH2 mutation in long-QT syndrome. *EMBO J* 32(24):3161–3175.
7. Costa M, et al. (2007) A method for genetic modification of human embryonic stem cells using electroporation. *Nat Protoc* 2(4):792–796.
8. Szuhai K, Tanke HJ (2006) COBRA: Combined binary ratio labeling of nucleic-acid probes for multi-color fluorescence in situ hybridization karyotyping. *Nat Protoc* 1(1): 264–275.
9. Takahashi K, Okita K, Nakagawa M, Yamanaka S (2007) Induction of pluripotent stem cells from fibroblast cultures. *Nat Protoc* 2(12):3081–3089.
10. Frank S, Zhang M, Schöler HR, Greber B (2012) Small molecule-assisted, line-independent maintenance of human pluripotent stem cells in defined conditions. *PLoS ONE* 7(7):e41958.
11. Dambrot C, et al. (2014) Strategies for rapidly mapping proviral integration sites and assessing cardiogenic potential of nascent human induced pluripotent stem cell clones. *Exp Cell Res* 327(2):297–306.
12. Müller FJ, et al. (2011) A bioinformatic assay for pluripotency in human cells. *Nat Methods* 8(4):315–317.
13. Barry PH, Lynch JW (1991) Liquid junction potentials and small cell effects in patch-clamp analysis. *J Membr Biol* 121(2):101–117.
14. Verkerk AO, Tan HL, Ravesloot JH (2004) $Ca^{2+}$-activated $Cl^-$ current reduces transmural electrical heterogeneity within the rabbit left ventricle. *Acta Physiol Scand* 180(3):239–247.
15. Hoekstra M, Mummery CL, Wilde AA, Bezzina CR, Verkerk AO (2012) Induced pluripotent stem cell derived cardiomyocytes as models for cardiac arrhythmias. *Front Physiol* 3:346.
16. Strutz-Seebohm N, et al. (2011) Structural basis of slow activation gating in the cardiac I Ks channel complex. *Cell Physiol Biochem* 27(5):443–452.
17. Seebohm G, et al. (2014) Structural basis of PI(4,5)P-dependent regulation of GluA1 by phosphatidylinositol-5-phosphate 4-kinase, type II, alpha (PIP5K2A). *Pflugers Archiv.* 66(10):1885–97.

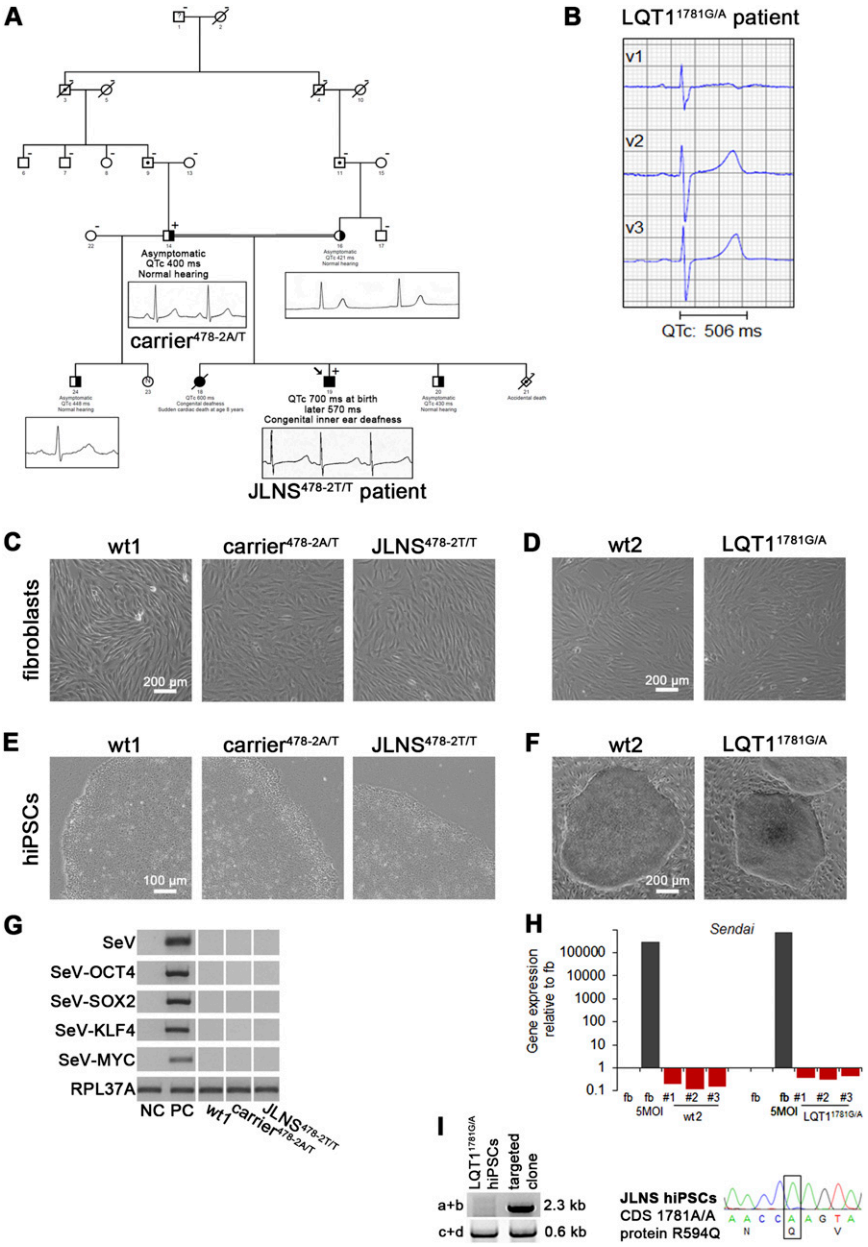


**Fig. S1.** Generation of hiPSCs from individuals with *KCNQ1* mutations. (*A*) Pedigree of the family with the carrier$^{478\text{-}2A/T}$ (#14) and the JLNS$^{478\text{-}2T/T}$ patient (#19) with the heterozygous and homozygous c.478-2A>T *KCNQ1* mutation, respectively. ECG of the JNLS patient shows a prolonged QT interval (QTc: 570 ms). This patient has congenital inner ear deafness. The heterozygous carrier is asymptomatic with a normal QTc (400 ms). JLNS patients are indicated by filled symbols, heterozygous mutation carriers are shown as half-filled symbols. Circles represent female; squares male family members. "-" indicates no DNA available. The arrow indicates the proband. (*B*) ECG of the LQT1$^{1781G/A}$ patient with the c.1781G>A *KCNQ1* mutation, showing a prolongation of the QTc interval of 506 ms (normal QTc ≤460 ms). (*C* and *D*) Primary fibroblasts obtained from skin biopsies of the indicated individuals. (*E* and *F*) Morphology of representative reprogrammed hiPSC colonies. (*G*) RT-PCR analysis of Sendai viral vector in hiPSCs. (*H*) qPCR analysis of Sendai viral vector in three independent clones from the wt2 and the LQT1$^{1781G/A}$ lines. All values are normalized to *GAPDH* and are relative to parental fibroblasts (fb). (*I*, *Left*) PCR analysis for identifying targeted hiPSC clones (a+b, 2.3 kb) and for confirming the introduction of the mutation (c+d, 0.6 kb). (*I*, *Right*) Sequencing of a clonally isolated hiPSC line confirming the conversion into the homozygous mutated genotype.

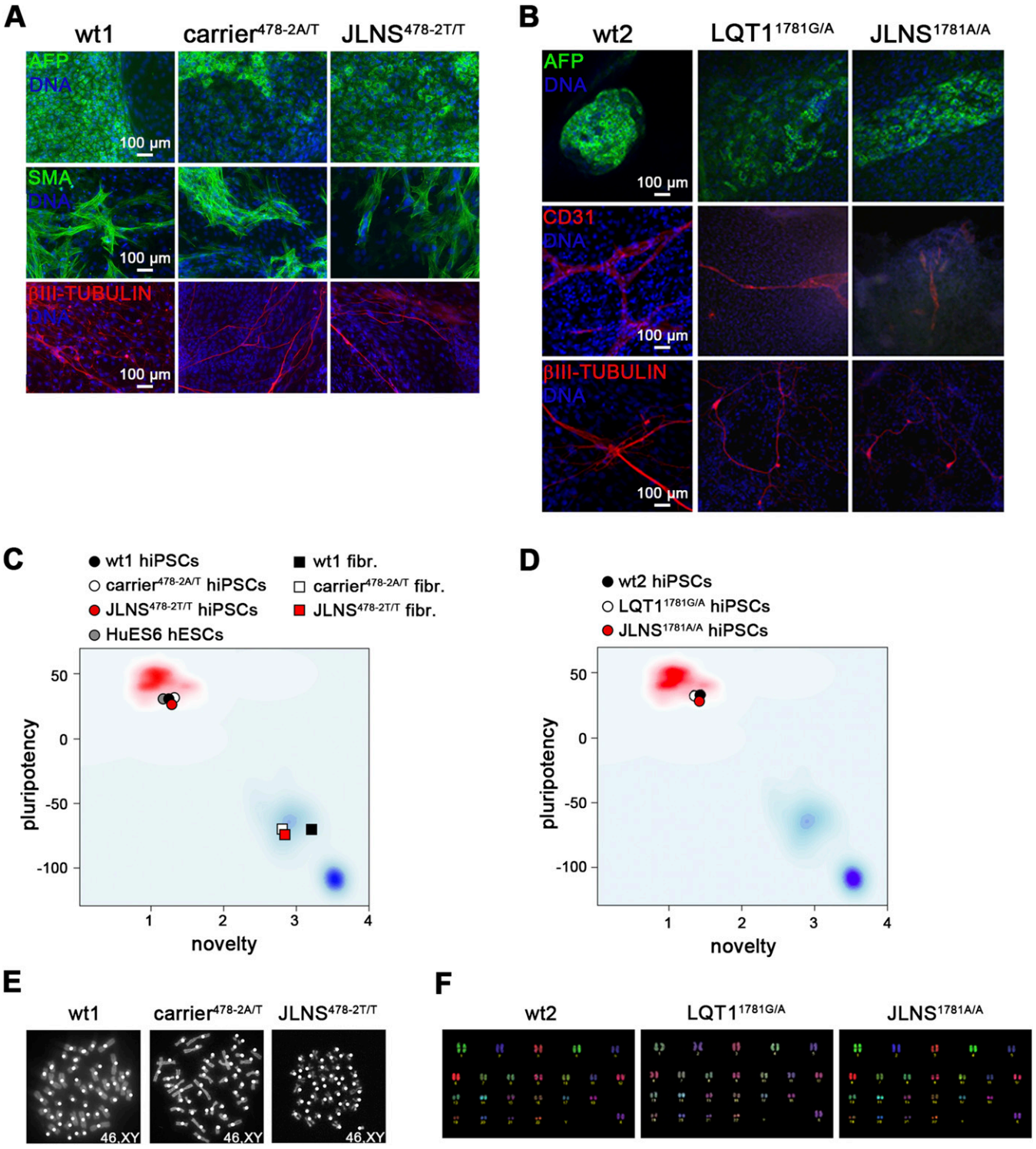


**Fig. S2.** hiPSCs are pluripotent and have a normal karyotype. (*A* and *B*) Immunofluorescence analysis of germ-layer markers after hiPSC spontaneous differentiation; AFP, endoderm; CD31 and SMA, mesoderm; βIII-TUBULIN, ectoderm. (*C* and *D*) PluriTest analysis of the indicated hiPSCs, parental fibroblasts, and hESCs. All lines have a high "pluripotency score" and a low "novelty score," indicating that they show global gene expression profiles similar to hESCs. (*E* and *F*) All hiPSCs have a normal karyotype. White dots mark individual chromosomes (*E*).

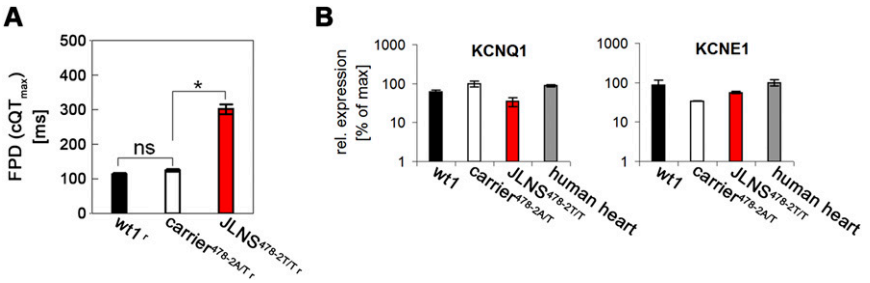


**Fig. S3.** FPD phenotype and *KCNQ1* and *KCNE1* expression in hiPSCs. (*A*) FPD analysis in wt1$^{r}$-, carrier$^{478\text{-}2A/T\ r}$-, and JLNS$^{478\text{-}2T/T\ r}$-CMs derived from independent sets of retrovirally ("r") reprogrammed hiPSCs ($n = 30$ each). ns, not significant. *$P < 0.05$. (*B*) qPCR analysis of *KCNQ1* and *KCNE1* in CMs from the indicated hiPSC lines. Human heart biopsy tissue is shown as a reference.

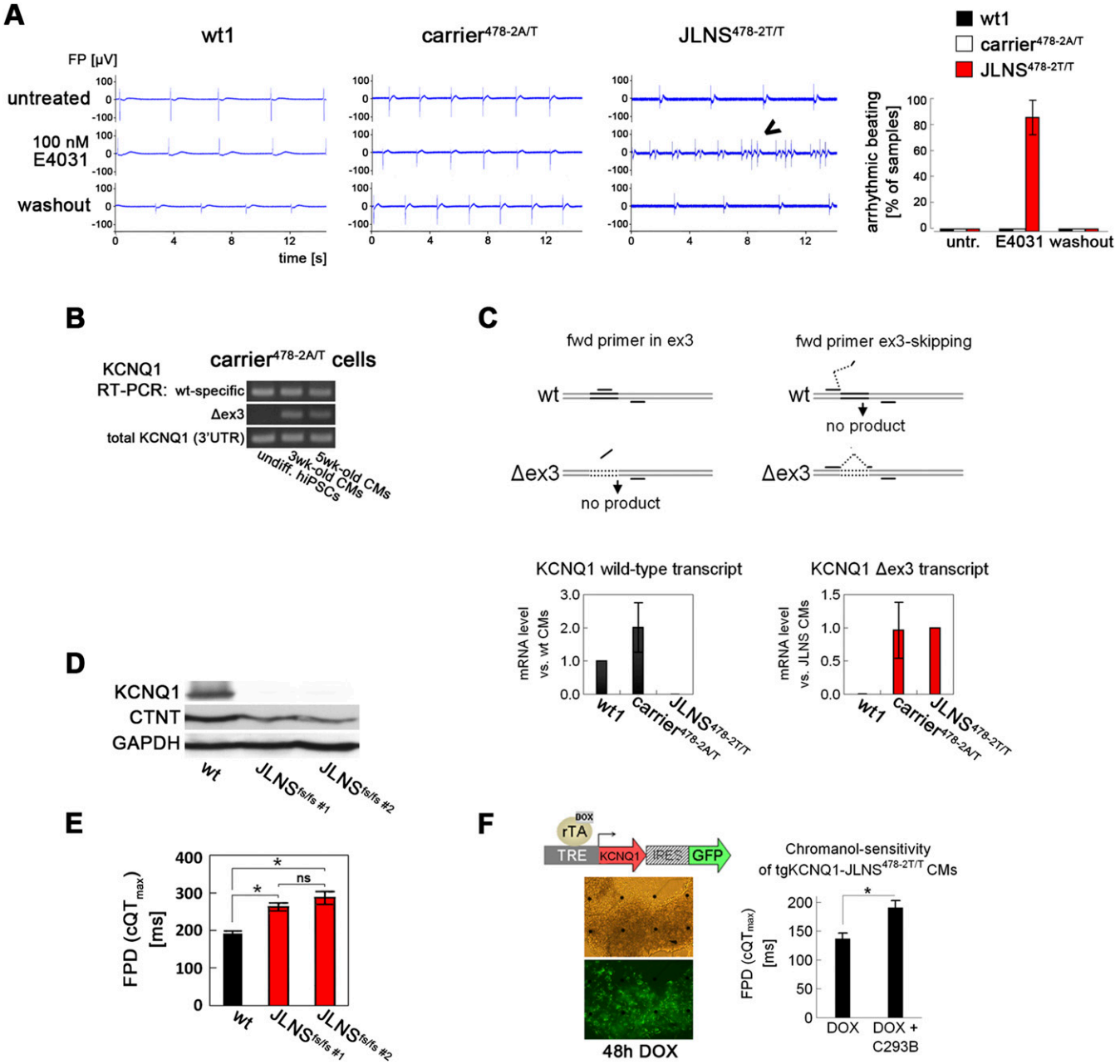


**Fig. S4.** Analysis of the electrophysiological and molecular mechanisms of action of the c.478-2A>T *KCNQ1* mutation in hiPSC-CMs. (*A*) Representative MEA recordings showing effects of the hERG inhibitor E4031. Arrhythmia is visible only in JLNS$^{478\text{-}2T/T}$-CMs (100 nM E4031). (*A, Right*) Quantification of arrhythmic beatings ($n$ = 4–7). (*B*) Loss of *KCNQ1* imprinting in carrier$^{478\text{-}2A/T}$-CMs, using isoform-specific primers illustrated in *C*. Undifferentiated hiPSCs display mono-allelic expression of the wt *KCNQ1* allele (wt-specific only). (*C*) Schematic of qPCR-based detection of wt and Δex3 *KCNQ1* mRNA (*Top*). wt *KCNQ1* transcript is expressed at similar levels in wt1- and carrier$^{478\text{-}2A/T}$-CMs but is absent in JLNS$^{478\text{-}2T/T}$-CMs (*Bottom Left*). Δex3 *KCNQ1* transcript is absent in wt1-CMs (*Bottom Right*). (*D* and *E*) Western blot analysis using an antibody detecting the C terminus of KCNQ1 (*D*) and FPD quantification ($n$ = 5) (*E*), in CMs derived from wt- and two independent engineered JLNS$^{fs/fs}$-hESCs (JLNS$^{fs/fs\ \#1}$ and JLNS$^{fs/fs\ \#2}$). ns, not significant. (*F*) Phenotypic rescue of JLNS$^{478\text{-}2T/T}$-CMs using *KCNQ1* transgene delivery. Shown are PiggyBac vector illustration (*Top Left*); transgenic DOX-treated JLNS$^{478\text{-}2T/T}$-CMs plated on MEA (*Bottom Left*); FPD quantification showing gain of C293B sensitivity in DOX-treated transgenic JLNS$^{478\text{-}2T/T}$-CMs (*Right*, $n$ = 4). *$P$ < 0.05.

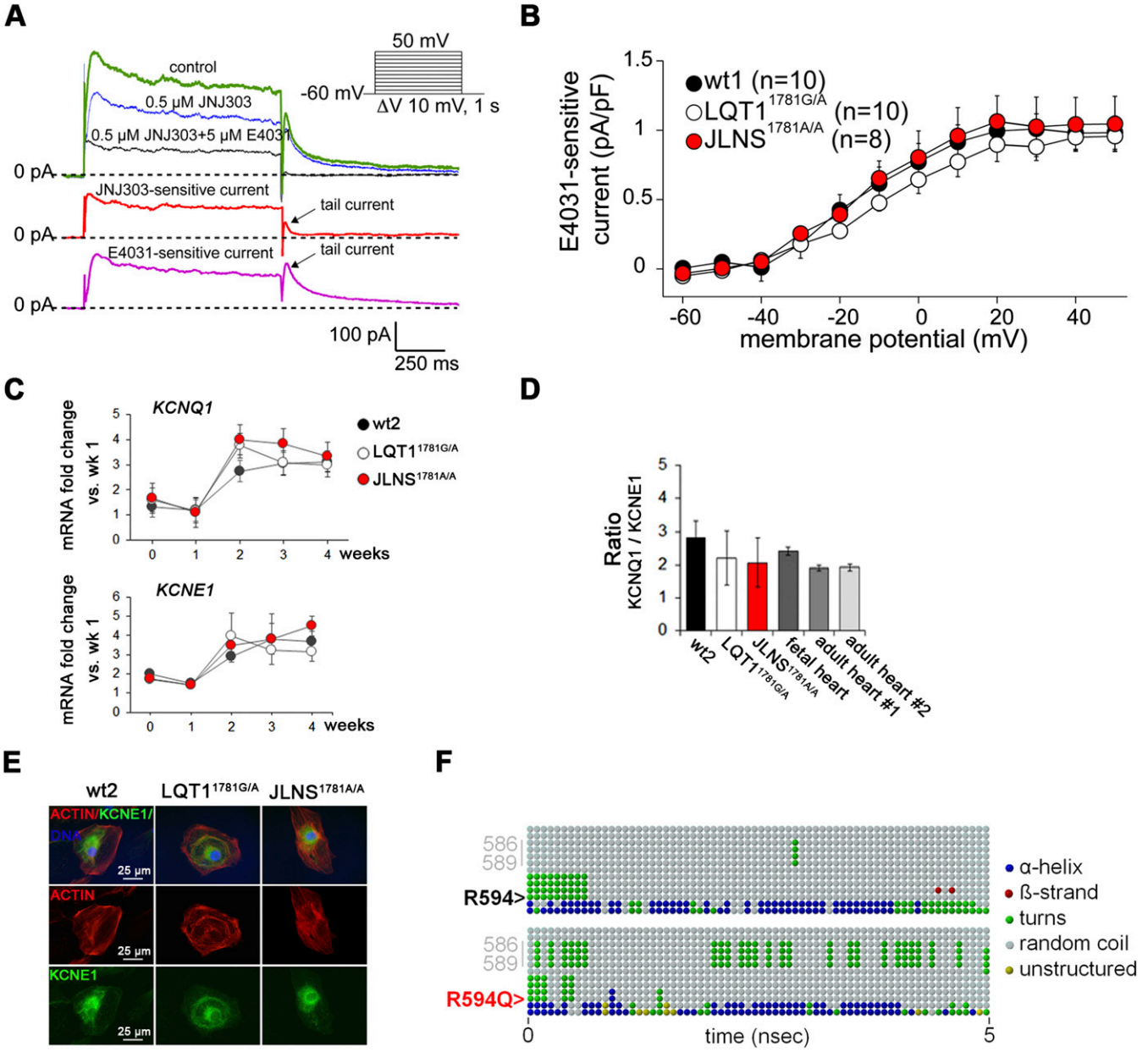


**Fig. S5.** Analysis of the electrophysiological and molecular mechanisms of action of the c.1781G>A *KCNQ1* mutation in hiPSC-CMs. (*A*) Representative traces showing the protocols for measuring $I_{Ks}$ and $I_{Kr}$. $I_{Ks}$ is measured as 0.5 μM JNJ303-sensitive current, whereas $I_{Kr}$ is measured as 5 μM E4031-sensitive current. The arrows indicate tail currents. (*Inset*) voltage protocol. (*B*) Average E4031-sensitive tail currents in hiPSC-CMs. $I_{Kr}$ is similar in all three lines. (*C*) qPCR time-course analysis of *KCNQ1* and *KCNE1* expression during cardiac differentiation in wt2, LQT1$^{1781G/A}$, and JLNS$^{1781A/A}$ hiPSCs. Values are normalized to *GAPDH* and relative to 1-wk differentiated cells ($n = 2$). (*D*) qPCR analysis of *KCNQ1*/*KCNE1* ratio in hiPSC-CMs. Human fetal and adult heart tissues are shown as a reference. Values are normalized to *TNNT2* ($n = 3$). (*E*) Immunofluorescence analysis of KCNE1 (green) in hiPSC-CMs. ACTIN is shown in red by phalloidin staining, and nuclei are stained in blue. (*F, Upper*) Molecular dynamics simulation of a peptide surrounding KCNQ1 amino acid residue 594. (*F, Bottom*) The wt R amino acid has been mutated into Q (R594Q). The mutation induces local structure changes. Colored dots represent secondary structure elements.

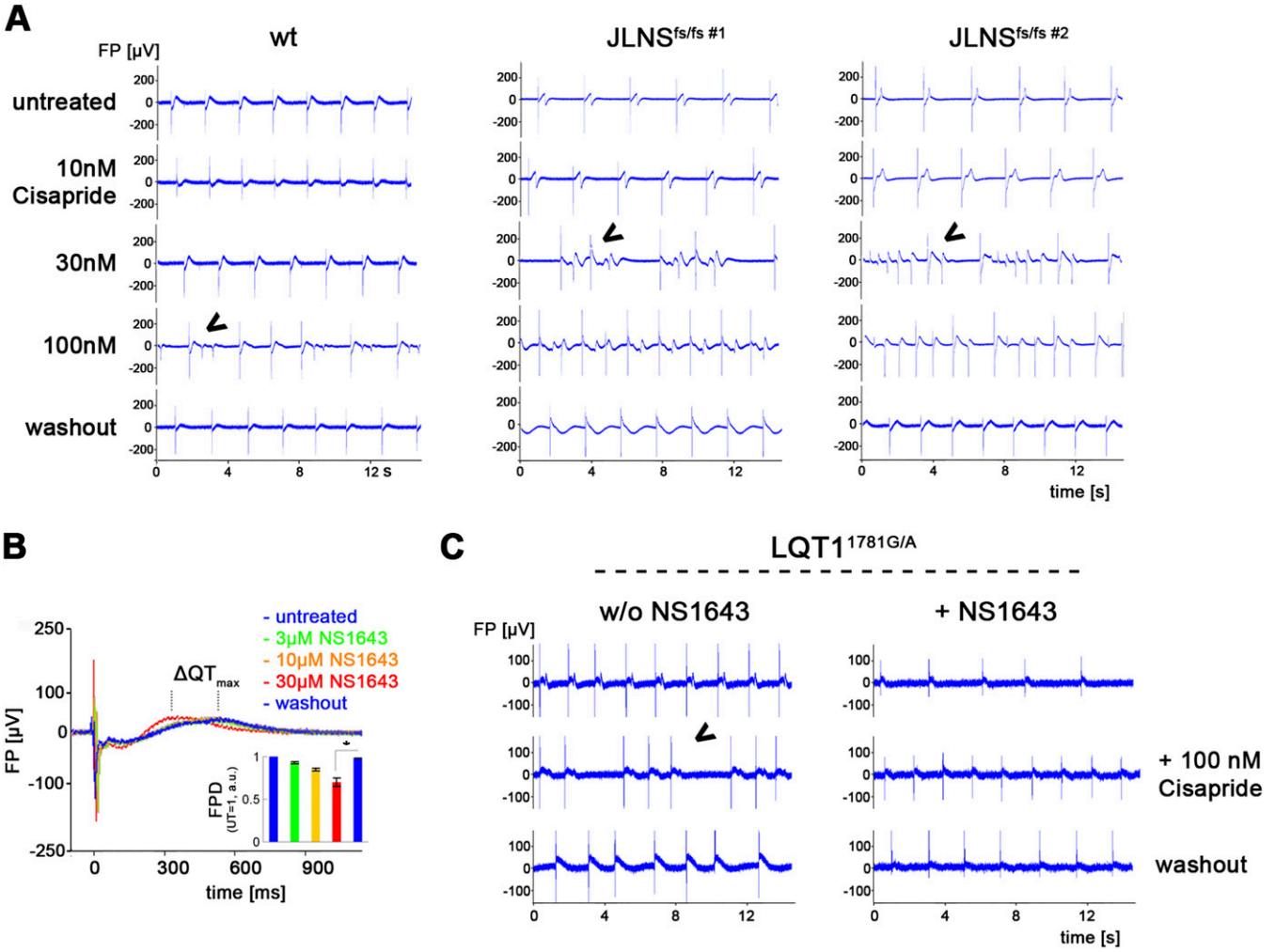


**Fig. S6.** Drug-induced arrhythmia phenotypes in hiPSC- and hESC-CMs and rescue by NS1643. (*A*) Cisapride causes arrhythmias in spontaneously beating isogenic wt- and JLNS$^{fs/fs}$-CMs. Representative MEA traces are shown. Arrowheads indicate first appearance of arrhythmia. (*B*) The $I_{Kr}$ activator NS1643 reduces FPD in wt1-CMs in a dose-dependent manner. Representative MEA traces and relative FPD quantification ($n = 2$) are shown. (*C*) Pretreatment with the hERG channel activator NS1643 (30 µM) protects LQT1$^{1781A/A}$-CMs from high-dose Cisapride induced arrhythmia. Representative MEA traces from independent experiments are shown.

**Table S1. Primers used for genotyping, cloning, screening for targeted clones, RT-PCR, and qPCR**

| Gene/name | Fwd primer | Rev primer |
|---|---|---|
| Primers for qPCR | | |
| OCT4 | GACAGGGGGAGGGGAGGAGCTAGG | CTTCCCTCCAACCAGTTGCCCCAAAC |
| ATP2A2 | TCACTGCGCATGTTTGACTTTAGA | TGTCTGTGCGACGCTCATTG |
| CACNA1C | CCAGGCTCCACGACTTCACA | GGCCTTTCTCGAGGGTGAGA |
| CACNA1C | CAATCTCCGAAGAGGGGTTT | TCGCTTCAGACATTCCAGGT |
| GAPDH | TCCTCTGACTTCAACAGCGA | GGGTCTTACTCCTTGGAGGC |
| HERG/KCNH2 | CGGTGCATGTGTGGTCTTGA | TGACATCTGCCTGCACCTGA |
| KCND3 | CCAATTCTAACCTGCCAGCTAC | CTGCTTTCAAATTAAGGCTGGA |
| KCNE1 | CAGGCACACGGACTGGCTATT | GCCTGGGAAGACTAACGCCATA |
| KCNE1 | TCTCTGGCCAGTTTCACACA | CTCAAACTTCCCAGGCACAC |
| KCNE2 | TGTGTGCAACCCAGAAGAGA | CTTCCAGCGTCTGTGTGAAA |
| KCNH2 | CACCGCCCTGTACTTCATCT | AGGCCTTGCATACAGGTTCA |
| KCNJ12 | TGGATCCTTTCCAGTTGGTG | CGGCTCCTCTTGAGTTCTATCTT |
| KCNQ1 | GCAGCCAGCCAAACACACA | GCGATGTAATGCCCAGAAGGA |
| KCNQ1 | TCCTGGTCTGCCTCATCTTC | AAGAACACCACCAGCACGAT |
| KCNQ1 wt | CATCGTCCTGGTCTGCCTCA | CCGAAGAACACCACCAGCAC |
| KCNQ1 Δex3 | CATCGTCCTGGTCTGCCTCA | CACGACCACGATGAGGTCATC |
| NANOG | CCTGTGATTTGTGGGCCTG | GACAGTCTCCGTGTGAGGCAT |
| NANOG | TGCAAGAACTCTCCAACATCCT | ATTGCTATTCTTCGGCCAGTT |
| OCT4 endo | GGAAGGAATTGGGAACACAAAGG | AACTTCACCTTCCCTCCAACCA |
| RPL37A | GTGGTTCCTGCATGAAGACAGTG | TTCTGATGGCGGACTTTACCG |
| RPS16 | GCTATCCGTCAGTCCATCTCCAA | CCTTCTTGGAAGCCTCATCCAC |
| RYR2 | GGAGCCAGTGTCATCCACCA | CAGGTGGCTGAAAGAATGAGCA |
| SCN5A | ACTGCACAATGACCAGCAGGA | GTGAGAAGTGCTCGATTAGTTCAGACA |
| SCN5A | GAGCTCTGTCACGATTTGAGG | GAAGATGAGGCAGACGAGGA |
| Sendai virus | ATGCAGCAGTACGTCACAGG | AGGCACTGCTGATCTTCGAT |
| SOX2 | GGGAAATGGGAGGGGTGCAAAAGAGG | TTGCGTGAGTGTGGATGGGATTGGTG |
| SOX2 endo | GCTCTTGGCTCCATGGGTTC | GCTGATCATGTCCCGGAGGT |
| TNNT2 | AGCATCTATAACTTGGAGGCAGAG | TGGAGACTTTCTGGTTATCGTTG |
| Primers for conventional RT-PCR | | |
| KCNQ1 span ex3 | ACCACTTCGCCGTCTTCCTC | GGAGAAGATGAGGCCCAGGA |
| RPL37A | TCCGCTCGTCCGCCTAATAC | TACCGTGACAGCGGAAGTGG |
| Sendai virus backbone | GGATCACTAGGTGATATCGAGC | ACCAGACAAGAGTTTAAGAGATATGTATC |
| SeV-KLF4 | TTCCTGCATGCCAGAGGAGCCC | AATGTATCGAAGGTGCTCAA |
| SeV-MYC | TAACTGACTAGCAGGCTTGTCG | TCCACATACAGTCCTGGATGATGATG |
| SeV-OCT4 | CCCGAAAGAGAAAGCGAACCAG | AATGTATCGAAGGTGCTCAA |
| SeV-SOX2 | ATGCACCGCTACGACGTGAGCGC | AATGTATCGAAGGTGCTCAA |
| Primers for conventional PCR on gDNA | | |
| KCNQ1 478–2 | ACCTGGGCTCCACTGCCTAT | TGGGAATCTGTGAGGGACCA |
| KCNQ1 CRISPR screen 1 | CTCCCTGTAAGGGCAAAGTG | TGACTCACCGATGATGGAAA |
| KCNQ1 CRISPR screen 2 | CACTGCCTATGGACATGAGCTGAA | TGACTCACCGATGATGGAAA |
| KCNQ1 G1781A (c+d) | AGTGTGGCCAGCTTAGGCAG | ACAAAGCAGACTACGAGAGG |
| KCNQ1 (a+b) | CTGGGTTCTGTACGCTCCTG | CACCTAACTAGCTGTGTGAC |
| Primers for cloning | | |
| KCNQ1 rs1057128 | CTTCGCCGAGGACCTGGACCTG | GATCAACAGTGAGGGCTTCC |
| KCNQ1 span ex3 cl | CCCAGGGCCGAGAGGAAG | GGATCTGCAGGAAGCGGATG |
| KCNQ1 full cl | TACGCGTGGAATTCGATCTAGCACCAT | TACTAGTTCAGGACCCCTCATCG |
| KCNQ1 CRISPR 1 | CACCGCTGGTGGTGTTCTTCGGGA | AAACTCCCGAAGAACACCACCAGC |
| KCNQ1 CRISPR 2 | CACCGATCTCCTGCAGGGACAGAG | AAACCTCTGTCCCTGCAGGAGATC |
| KCNQ1 Neo | CCCATGGCCTGGGGCGGCCGTGGGGCCC-TGAGACCAGCAAATTGGGTCATCACT | CACAGCCCCATGGGGCCAGGCACCTGA-ACACCAGCCTTCGCTCTTTCTGCAGCTCGG |
| KCNQ1 targeting vector (subcloning step) | CGCAGATCCAGGGGCCTCCTCACAGCGAGTC-TACTTCCTGCGGGCCTCCCTTAATTAATC | GCGCTTGGGAAAGTAGGGGCTACAGGACAAAT-TAACAAGGGAAAGTTGCCGCGG... |
| KCNQ1 G1781A | CGCCCGCCTGAACCAAGTAGAAGACAAGG | CCTTGTCTTCTACTTGGTTCAGGCGGGCG |